Journal of Power Sources 213 (2012) 10–15

Contents lists available at SciVerse ScienceDirect

Journal of Power Sources

journal homepage: www.elsevier.com/locate/jpowsour

High-capacity $Li_2Mn_{0.8}Fe_{0.2}SiO_4$/carbon composite nanofiber cathodes for lithium-ion batteries

Shu Zhang, Ying Li, Guanjie Xu, Shuli Li, Yao Lu, Ozan Toprakci, Xiangwu Zhang*

Fiber and Polymer Science Program, Department of Textiles Engineering, Chemistry and Science, North Carolina State University, Raleigh, NC 27695-8301, USA

ARTICLE INFO

Article history:
Received 25 February 2012
Received in revised form
4 April 2012
Accepted 5 April 2012
Available online 13 April 2012

Keywords:
Li_2MnSiO_4
Iron doping
Cathode
Electrospinning
Carbon nanofibers

ABSTRACT

Li_2MnSiO_4 has been considered as a promising cathode material with an extremely high theoretically capacity of 332 mAh g^{-1}. However, due to its low intrinsic conductivity and poor structural stability, only about half of the theoretical capacity has been realized in practice and the capacity decays rapidly during cycling. To realize the high capacity and improve the cycling performance, $Li_2Mn_{0.8}Fe_{0.2}SiO_4$/carbon composite nanofibers were prepared by the combination of iron doping and electrospinning. X-ray diffraction, scanning electron microscope, and transmission electronic microscope were applied to characterize the $Li_2Mn_{0.8}Fe_{0.2}SiO_4$/carbon nanofibers. It was found that $Li_2Mn_{0.8}Fe_{0.2}SiO_4$ nanoparticles were embedded into continuous carbon nanofiber matrices, which formed free-standing porous mats that could be used as binder-free cathodes. The iron doping improved the conductivity and purity of the active material, and the carbon nanofiber matrix facilitated ion transfer and charge diffusion. As a result, $Li_2Mn_{0.8}Fe_{0.2}SiO_4$/carbon nanofiber cathodes showed promising improvement on reversible capacity and cycling performance.

1. Introduction

Among various known cathode materials for Li-ion batteries, $LiCoO_2$, $LiMn_2O_4$ and $LiNiO_2$ have been most widely studied. Recently, $LiFePO_4$ provided an alternative for cathode materials with higher thermal stability and environmental benign nature [1,2]. $LiFePO_4$ has a theoretical capacity of 170 mAh g^{-1}; however, with the emerging high demand of Li-ion batteries for providing electricity in hybrid electric vehicles and storing energy in power grids, it falls short to offer sufficient specific capacity and energy density. Dominko [3] firstly synthesized and characterized a new material Li_2MnSiO_4 with the possibility to deliver two lithium ions per formula unit, leading to a theoretical capacity of 333 mAh g^{-1}. However, only less than one lithium ion per formula unit has been realized in practice, and serious capacity loss was also observed during cycling [3]. The poor conductivity (5×10^{-16} S cm^{-1}) and slow kinetics of Li_2MnSiO_4 are probably the main reason why researchers have not been able to extract more than one lithium ion per formula unit [4]. To circumvent the low electronic conductivity and slow kinetics of the lithium orthosilicate, several methods were employed including size reduction [3], carbon coating [5], and super-valent metal doping [6]. Although progress has been made by these methods, the overall performance of Li_2MnSiO_4 is still not sufficient for practical battery applications.

Electrospinning is considered as a simple but versatile strategy to fabricate various inorganic materials such as titanium oxide [7] and $LiFePO_4$ [8,9], and organic polymeric nanofibers as well. Herein, we report a novel approach for the synthesis of $Li_2Mn_{0.8}Fe_{0.2}SiO_4$/carbon composite nanofibers by iron doping and electrospinning to incorporate both advantages of structure optimization and electronic/ionic conductivity enhancement. Electrochemical results show that $Li_2Mn_{0.8}Fe_{0.2}SiO_4$/carbon nanofiber cathodes exhibited promising improvement in terms of reversible capacity and cycling performance.

2. Experimental

2.1. Chemicals

N,N-dimethylformaamide (DMF), manganese (II) acetate (98%), citric acid (>99.5%), and ethylene glycol (99%) were purchased from Sigma–Aldrich Chemical Company Inc (USA). Polyacrylonitrile (PAN, Mw = 150,000) was ordered from Pfaltz & Bauer Inc. Lithium acetate dihydrate (98%), iron acetate (98%), and tetraethyl orthosilicate (98%) were obtained from Acros Organics. Electrolyte composited of 1 mol of lithium hexafluorophosphate ($LiPF_6$) in

* Corresponding author. Tel.: +1 919 515 6547; fax: +1 919 515 6532.
E-mail address: xiangwu_zhang@ncsu.edu (X. Zhang).

0378-7753/$ – see front matter © 2012 Elsevier B.V. All rights reserved.
doi:10.1016/j.jpowsour.2012.04.011

a mixture solution of ethylene carbonate (EC), diethyl carbonate (DEC), and dimethyl carbonate (DMC) with a volume ratio of 1:1:1 was purchased from MTI corporation. All materials were used as-received without further purification.

2.2. Preparation of $Li_2Mn_{0.8}Fe_{0.2}SiO_4$ powder

$Li_2Mn_{0.8}Fe_{0.2}SiO_4$ was prepared by a citric acid-assisted sol–gel Pechini method [3]. The synthesis was carried out by firstly dissolving lithium acetate, manganese acetate, and iron acetate with a molar ratio of 2.0:0.8:0.2 in distilled water under vigorous stirring for 2 h. A saturated aqueous solution of citric acid and ethylene glycol complexation agents with a ratio of 2:1 was then slowly added into the above mixture under continuous stirring. After 12 h, a homogenous solution was formed, and then it was transferred into a reflux system. Tetraethyl orthosilicate in ethanol was then added to the system by about one drop per minute, and the solution was maintained at 80 °C under magnetic stirring during the entire process. A greenish solution was formed and it was kept at 75 °C to form a wet gel. The gel was vacuum-dried at 100 °C and was then ground with mortar and pestle. The obtained mixture was heat treated in a furnace at 700 °C for 12 h in flowing argon. The resultant $Li_2Mn_{0.8}Fe_{0.2}SiO_4$ product was ground with mortar and pestle again for at least 1 h. For comparison, Li_2MnSiO_4 powder was also prepared using the same method.

2.3. Fabrication of $Li_2Mn_{0.8}Fe_{0.2}SiO_4$/carbon composite nanofibers

PAN was used as the carbon source and electrospinning media. The electrospinning solution was prepared by mixing the obtained $Li_2Mn_{0.8}Fe_{0.2}SiO_4$ powder with an 8 wt% PAN solution in DMF. The content of $Li_2Mn_{0.8}Fe_{0.2}SiO_4$ was 65 wt% of the total mixture solution. A high voltage power supply (Gamma ES40P-20W/DAM) was used to provide a high voltage at around 20 kV for electrospinning. Fibers were collected on an aluminum plate as a mat. The electrospun $Li_2Mn_{0.8}Fe_{0.2}SiO_4$/PAN nanofibers were firstly stabilized in air environment at 280 °C for 5 h with a heating rate of 5 °C/min, and then carbonized at 700 °C for 8 h with a heating rate of 2 °C/min in high purity argon atmosphere. The content of carbon in $Li_2Mn_{0.8}Fe_{0.2}SiO_4$/carbon nanofiber composite sample was 19.8 wt %, as evaluated by CHN elemental analysis.

2.4. Nanofiber characterization

The morphology of $Li_2Mn_{0.8}Fe_{0.2}SiO_4$/carbon nanofibers were evaluated by scanning electron microscopy (JEOL 6400 FESEM at 20 kV) and transmission electron microscopy (Hitach HF-2000 TEM at 200 kV). The structure of $Li_2Mn_{0.8}Fe_{0.2}SiO_4$/carbon nanofibers was also characterized using X-ray diffraction (Rigaku Smartlab).

2.5. Electrochemical evaluation

Electrochemical tests were performed using 2032 coin-type half cells. The $Li_2Mn_{0.8}Fe_{0.2}SiO_4$/carbon nanofiber mats were cut into circular electrodes by a punch of 1/2 inch in diameter. Li sheet was used as the counter electrode, and polypropylene (PP) film (Celgard 2400) as the separator. The electrolyte used was 1 M solution of $LiPF_6$ in an EC/DMC/DEC mixture (1:1:1 by volume). The cell assembly process was carried out under dry argon atmosphere in a glove box. Charge and discharge were conducted on a Land battery testing system at a current density of C/20 between cut-off potentials of 2.0 and 4.8 V. For comparison, electrodes made from Li_2MnSiO_4 and $Li_2Mn_{0.8}Fe_{0.2}SiO_4$ powders were also prepared and tested by mixing powders with 10 wt% polyvinylidene fluoride (PVdF) binder and 10 wt% conducting carbon black and casting on aluminum current collector. The specific capacities were calculated based on the weight of $Li_2Mn_{0.8}Fe_{0.2}SiO_4$.

3. Results and discussion

3.1. X-ray diffraction

The X-ray diffraction patterns obtained from Li_2MnSiO_4 and $Li_2Mn_{0.8}Fe_{0.2}SiO_4$ powders are presented in Fig. 1. Both Li_2MnSiO_4 and $Li_2Mn_{0.8}Fe_{0.2}SiO_4$ powders have the orthorhombic crystal structure and the space group is $Pmn2_1$. Without iron doping, Li_2MnSiO_4 has a large diffusion peak at $2\theta = 41°$, which can be assigned to MnO as an impurity. However, this impurity peak cannot be observed in iron-doped $Li_2Mn_{0.8}Fe_{0.2}SiO_4$, indicating that the iron doping can improve the purity of active material.

3.2. Morphology and structure

Fig. 2 shows SEM images of Li_2MnSiO_4 and $Li_2Mn_{0.8}Fe_{0.2}SiO_4$ powders. Both Li_2MnSiO_4 and $Li_2Mn_{0.8}Fe_{0.2}SiO_4$ powders consist of agglomerated nanoparticles. For Li_2MnSiO_4, the primary particle diameter ranges from 30 to 50 nm. Iron doping decreases the particle size, and the primary particle diameter of $Li_2Mn_{0.8}Fe_{0.2}SiO_4$ powder is 15–30 nm. In addition, the particle distribution of $Li_2Mn_{0.8}Fe_{0.2}SiO_4$ powder is more uniform than that of Li_2MnSiO_4.

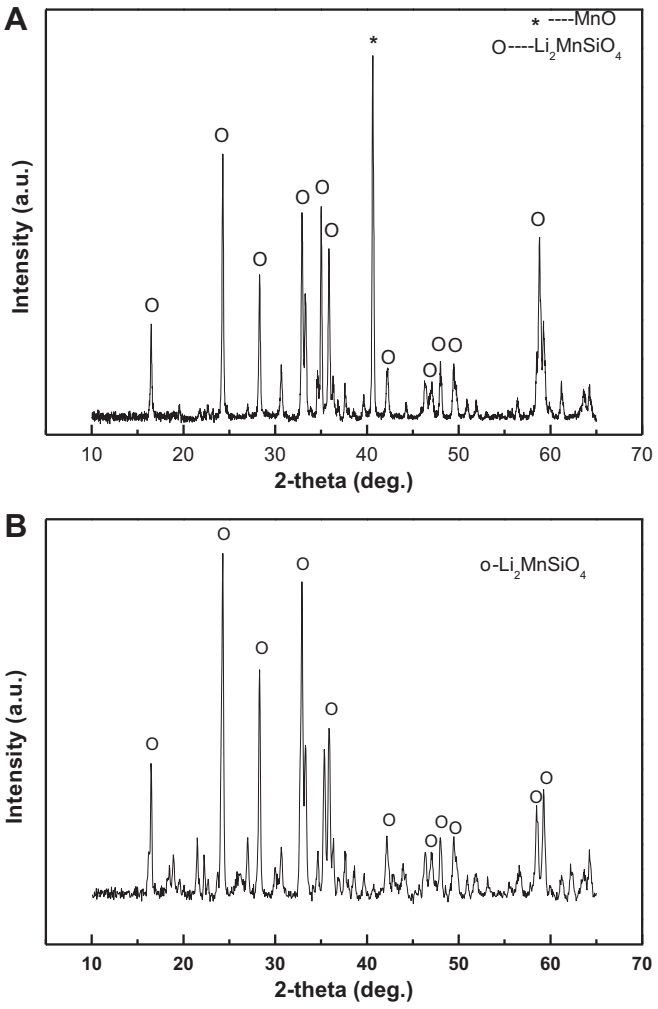

Fig. 1. XRD patterns of (A) Li_2MnSiO_4 and (B) $Li_2Mn_{0.8}Fe_{0.2}SiO_4$ powders.

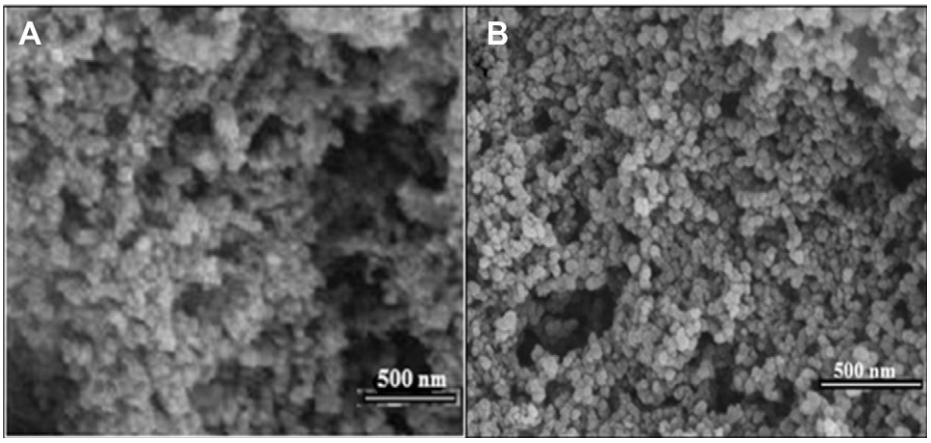

Fig. 2. SEM images of (A) Li_2MnSiO_4 and (B) $Li_2Mn_{0.8}Fe_{0.2}SiO_4$ powders.

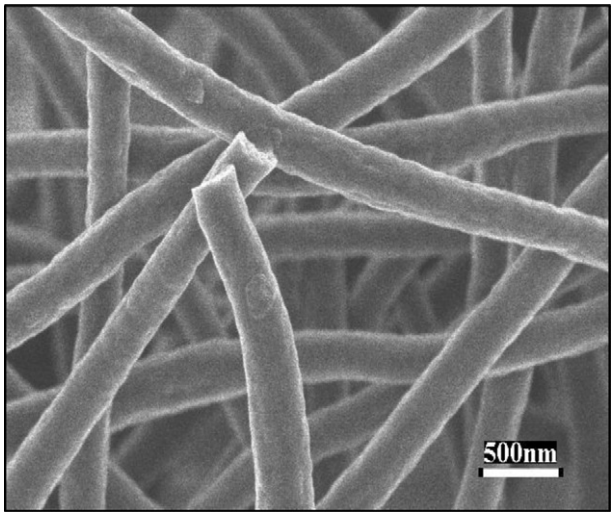

Fig. 3. SEM images of electrospun $Li_2Mn_{0.8}Fe_{0.2}SiO_4$/PAN nanofibers.

Fig. 3 shows SEM images of $Li_2Mn_{0.8}Fe_{0.2}SiO_4$/PAN electrospun nanofibers. They exhibit a continuous fibrous morphology with relatively uniform diameter ranging from 160 to 230 nm. The randomly-aligned continuous fibers form a fibrous mat. The fiber surface is relatively rough probably due to the presence of active particles in the fibers.

SEM images of $Li_2Mn_{0.8}Fe_{0.2}SiO_4$/carbon nanofibers obtained after a thermal treatment of 700 °C in argon are presented in Fig. 4. After heat treatment, fibers become slimmer with diameters ranging from 76 to 158 nm. The diameter reduction is mainly caused by the removal of various species from PAN during the formation of carbon nanofiber matrix. Close-up images of the hybridization structure of $Li_2Mn_{0.8}Fe_{0.2}SiO_4$ particles with carbon nanofibers are shown in TEM images of Fig. 5. The TEM results confirm the formation of a $Li_2Mn_{0.8}Fe_{0.2}SiO_4$/carbon nanocomposite with $Li_2Mn_{0.8}Fe_{0.2}SiO_4$ particles dispersed both along and inside the carbon nanofibers. Aggregation of primary particles or 'beads-on-a-string' morphology as shown in Fig. 5C can be only observed in a few small areas.

3.3. Raman analysis

The Raman spectrum of $Li_2Mn_{0.8}Fe_{0.2}SiO_4$/carbon nanofibers in the spectral region of 1100–2000 cm^{-1} was obtained (Fig. 6). Common Raman features of carbon materials are the presence of two strong bands at around 1350 and 1600 cm^{-1}, respectively. The strong peak centered near 1350 cm^{-1} (D-band) is characteristic of defect-induced structures of sp^3 structural disorder in the graphene layers of carbon materials, while the peak at 1600 cm^{-1} (G-band) is

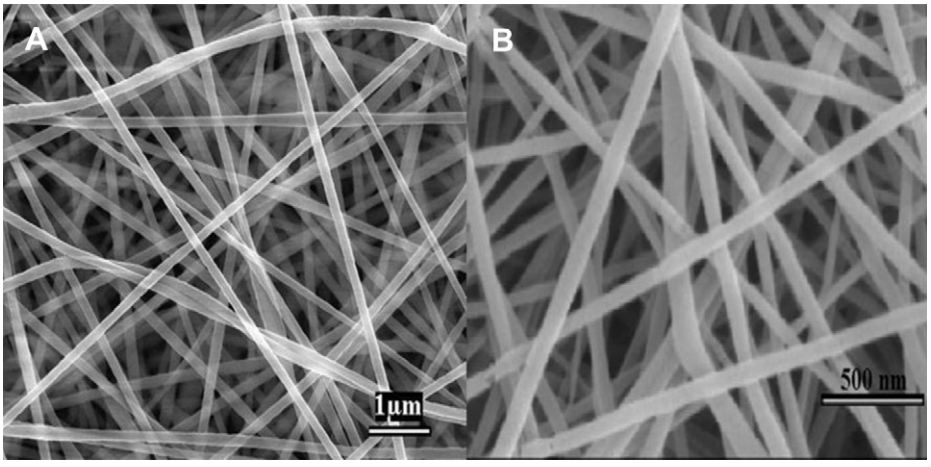

Fig. 4. SEM images of $Li_2Mn_{0.8}Fe_{0.2}SiO_4$/carbon nanofibers obtained after heat treatment.

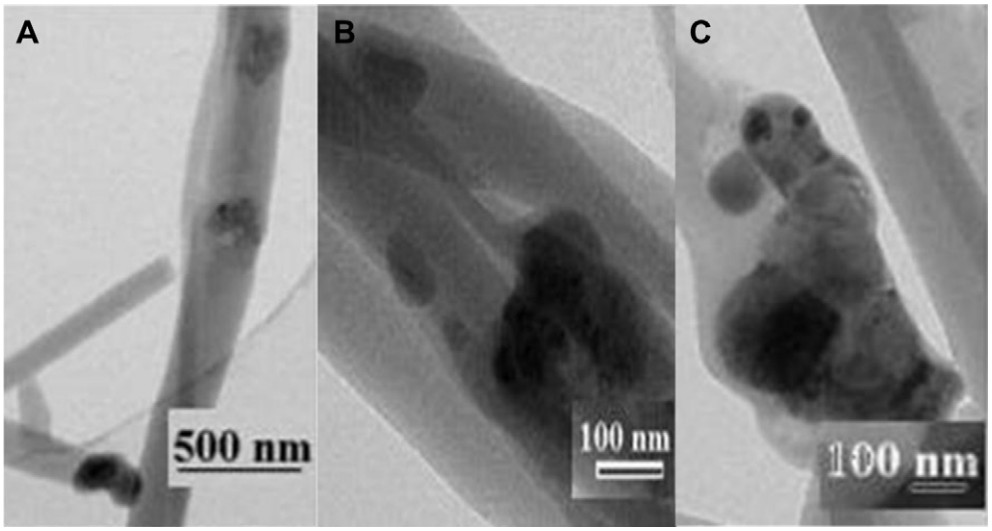

Fig. 5. TEM images of $Li_2Mn_{0.8}Fe_{0.2}SiO_4$/carbon nanofibers with magnifications of (A) 10,000× and (B and C) 30,000×.

indicative of the high-frequency E_{2g} first-order graphitic crystallites [10]. As shown in Fig. 6, the spectrum of $Li_2Mn_{0.8}Fe_{0.2}SiO_4$/carbon nanofibers clearly indicates the presence of both D band and G band, and hence the carbon nanofiber matrix is composited of both disordered carbon and ordered graphene sheets. However, the intensity of G band is greater than that of D band, suggesting a good structural integrity.

3.4. Electrochemical properties

To evaluate the electrochemical performance of $Li_2Mn_{0.8}Fe_{0.2}SiO_4$/carbon nanofibers, charge–discharge cycles were conducted at room temperature between 2.0 and 5.0 V at a current density of C/20 (16.65 mA g^{-1}), and the results are shown in Fig. 7. For comparison, the charge–discharge curves of Li_2MnSiO_4 and $Li_2Mn_{0.8}Fe_{0.2}SiO_4$ powders are also shown. It is seen that Li_2MnSiO_4 powder presents a high discharge capacity of 212 mAh g^{-1} at the first cycle, corresponding to an electrode reaction of 1.27 electron transfer per formula unit. The discharge capacity of Li_2MnSiO_4 powder fades rapidly to less than one electron transfer per formula unit at the second cycle. Continuous capacity loss can be also observed after the second cycle. The capacity loss during cycling may be attributed to the intrinsic structural instability of Li_2MnSiO_4.

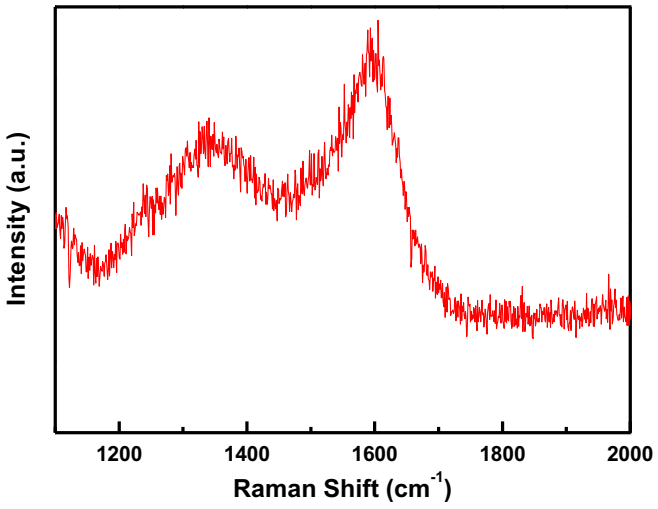

Fig. 6. Raman spectrum of $Li_2Mn_{0.8}Fe_{0.2}SiO_4$/carbon composite nanofibers.

After iron doping, the resultant $Li_2Mn_{0.8}Fe_{0.2}SiO_4$ powder give a higher initial discharge capacity of 220 mAh g^{-1} at the first cycle, indicating a 1.32 electrons exchange per formula unit. At the 10th cycle, the discharge capacity of $Li_2Mn_{0.8}Fe_{0.2}SiO_4$ powder is 170 mAh g^{-1}, demonstrating that the electrode reaction still remains at more than one electron transfer per formula unit.

By introducing the $Li_2Mn_{0.8}Fe_{0.2}SiO_4$ powder into carbon nanofiber matrix, the resultant $Li_2Mn_{0.8}Fe_{0.2}SiO_4$/carbon nanofibers show higher capacities and better capacity retention. For the first cycle, $Li_2Mn_{0.8}Fe_{0.2}SiO_4$/carbon nanofibers exhibit charge and discharge capacities of 233 mAh g^{-1} and 224 mAh g^{-1}, respectively. At the 20th cycle, the discharge capacity remains at 171 mAh g^{-1}, indicating a 1.02 electron transfer reaction per formula unit. In contrast, Li_2MnSiO_4 and $Li_2Mn_{0.8}Fe_{0.2}SiO_4$ powders show discharge capacities of 77 and 127 mAh g^{-1} at the 20th cycle. From Fig. 7, it is also seen that there are no apparent voltage steps in the charge–discharge curves. The absence of voltage steps is also found in Dominko's work [4]. This might be caused by the slow kinetics and structural change of Li_2MnSiO_4 during charge/discharge cycles. However, more work is needed to fully understand the actual mechanism.

Fig. 8 further compares the cycling performance of Li_2MnSiO_4 powder, $Li_2Mn_{0.8}Fe_{0.2}SiO_4$ powder, and $Li_2Mn_{0.8}Fe_{0.2}SiO_4$/carbon nanofibers. Among all three cathode materials, $Li_2Mn_{0.8}Fe_{0.2}SiO_4$/carbon nanofibers show the slowest capacity fading during cycling, with a capacity retention of 63.8% at the 50th cycle. The capacity retentions of Li_2MnSiO_4 and $Li_2Mn_{0.8}Fe_{0.2}SiO_4$ powders are only 20.5 and 41.3%, respectively, at the 50th cycle.

The improved electrical performance of $Li_2Mn_{0.8}Fe_{0.2}SiO_4$/carbon nanofibers can be attributed to the effect of iron doping and the formation of conductive carbon nanofiber matrix. For Li_2MnSiO_4 powder, the poor electrochemical performance can be partially attributed to its low conductivity. As reported by Dominko [11], the measured conductivity of Li_2FeSiO_4 is two orders of magnitude higher than that of Li_2MnSiO_4. It is anticipated that $Li_2Mn_{0.8}Fe_{0.2}SiO_4$ with super-valent ion doping has higher conductivity than Li_2MnSiO_4 [11]. In addition to the enhanced

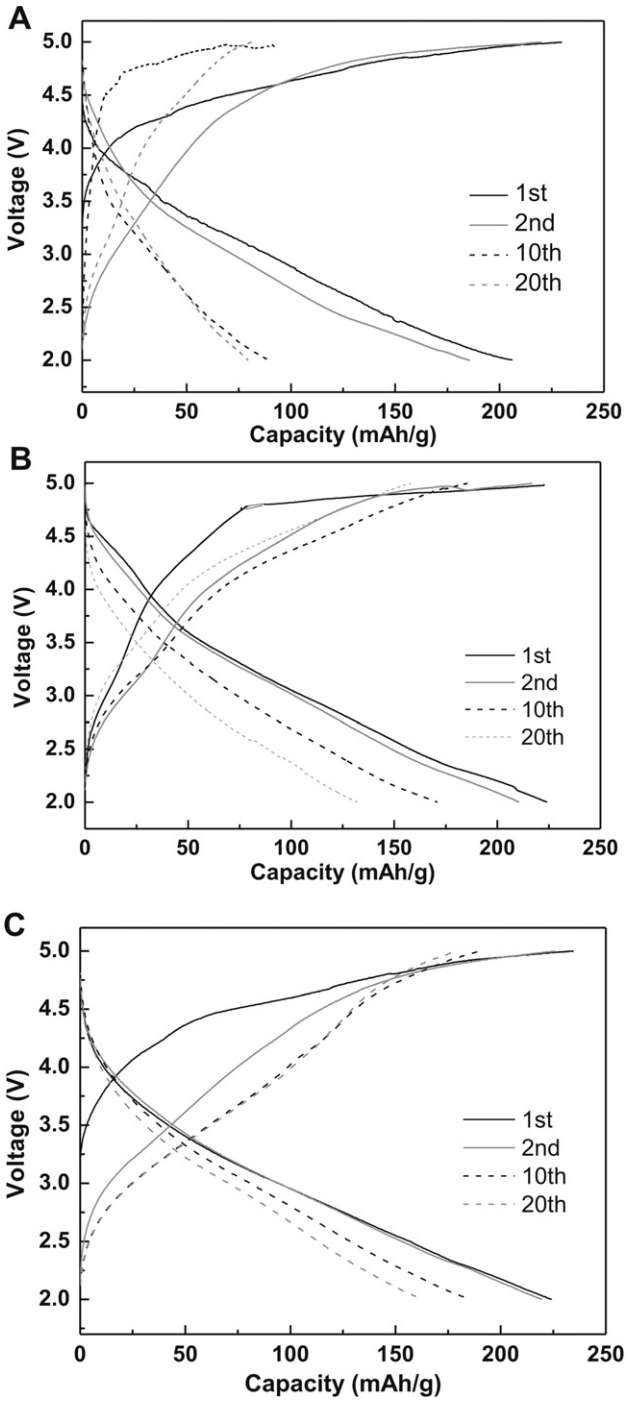

Fig. 7. Charge–discharge curves of (A) Li_2MnSiO_4 powder, (B) $Li_2Mn_{0.8}Fe_{0.2}SiO_4$ powder, and (C) $Li_2Mn_{0.8}Fe_{0.2}SiO_4$/carbon nanofibers.

conductivity, encapsulating active $Li_2Mn_{0.8}Fe_{0.2}SiO_4$ particles in the carbon nanofiber matrix keeps primary active particles from aggregation. The conductive carbon nanofiber matrix forms a three-dimensional porous network that can facilitate shorter transportation pathways for both lithium ions and electrons. The role of carbon nanofibers in improving the cycling performance and reversible capacities has been found in various electrode materials, including Si/carbon, Ni/carbon, $Li_4Ti_5O_{12}$/carbon, and $LiFePO_4$/carbon nanofiber electrodes [9,12–14]. The similar phenomenon was also observed in $LiMn_2O_4$/carbon nanotube cathodes [15].

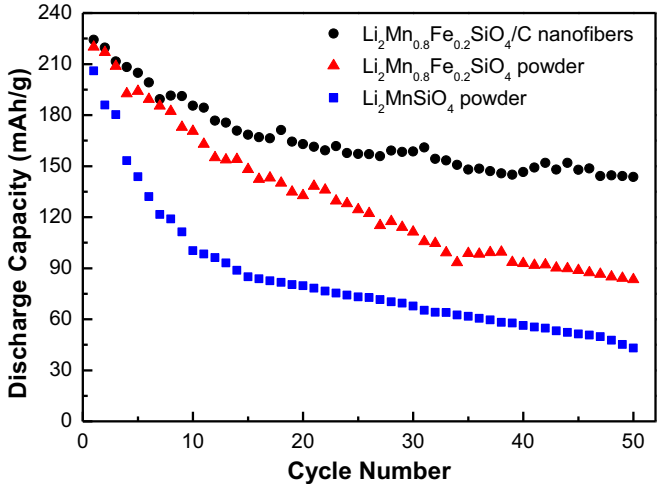

Fig. 8. Cycling performance of Li_2MnSiO_4 powder, $Li_2Mn_{0.8}Fe_{0.2}SiO_4$ powder, and $Li_2Mn_{0.8}Fe_{0.2}SiO_4$/carbon nanofibers.

Therefore, with combined advantages of enhanced conductivity resulted from iron doping and the improved electron and ion transportation due to the intimate networking of carbon nanofiber matrix, $Li_2Mn_{0.8}Fe_{0.2}SiO_4$/carbon composite nanofibers have improved electrochemical performance. However, more work is still needed to validate this mechanism.

However, the cycling performance of $Li_2Mn_{0.8}Fe_{0.2}SiO_4$/carbon nanofibers remains an issue as the capacity still fades too fast during cycling. The absence of voltage plateaus is also indicative of irreversible structural changes. Herein, more work should be devoted to further enhancement of the kinetics and cycling stability of this new cathode material.

4. Conclusions

In this work, a super-valent ion doping was carried out to form $Li_2Mn_{0.8}Fe_{0.2}SiO_4$, and both cyclability and capacity retention were improved. Especially, for the first ten cycles, discharge capacities from more than one electron transfer reaction were delivered. The $Li_2Mn_{0.8}Fe_{0.2}SiO_4$/carbon composite nanofibers were also prepared by a combination of electrospinning and heat treatment. The role of carbon fibers in the cathode material is mainly to facilitate fast transportation of electrons and lithium ions. This led to improved reversibility for $Li_2Mn_{0.8}Fe_{0.2}SiO_4$/carbon nanofibers. Results demonstrated that $Li_2Mn_{0.8}Fe_{0.2}SiO_4$/carbon nanofibers are as a promising high-capacity cathode material for Li-ion batteries.

Acknowledgments

The authors acknowledge the financial support of the National Textile Center, Advanced Transportation Energy Center, and ERC Program of the National Science Foundation under Award Number EEC-08212121.

References

[1] S.Y. Chung, Y.M. Bloking, Y.M. Chiang, Nature Materials 1 (2002) 123–128.
[2] O. Toprakci, H.A.K. Toprakci, L. Ji, KONA Powder and Particle Journal 28 (2010) 50–73.
[3] R. Dominko, M. Bele, A. Kokalj, M. Gaberscek, J. Jamnik, Journal of Power Sources 174 (2007) 457–461.
[4] R. Dominko, Journal of Power Sources 184 (2008) 462–468.

[5] Y. Li, Z. Gong, Y. Yang, Journal of Power Sources 174 (2007) 528–532.
[6] A. Kokalj, R. Dominko, G. Mali, A. Meden, M. Gaberscek, J. Jamnik, Chemistry of Materials 19 (2007) 3633–3640.
[7] N. Dharmaraj, H.C. Park, C.K. Kim, Y.K. Kim, D.R. Lee, Materials Chemistry and Physics 87 (2004) 5–9.
[8] F. Yheng-Wen, J. Ma, Q. Zong, Solid State Ionics 176 (2005) 1635–1640.
[9] O. Toprakci, L. Ji, Z. Lin, H.A.K. Toprakci, X. Zhang, Journal of Power Sources 196 (2011) 7692–7699.
[10] C. Kim, Y.I. Jeong, B.T. Ngoc, K.S. Yang, M. Kojima, Y.A. Kim, Small 3 (1) (2007) 91–95.
[11] M.E. Dompablo, U. Amador, J.M. Gallardo-Amores, E. Moran, H. Eharenberg, L. Dupont, R. Dominko, Journal of Power Sources 189 (2009) 638–642.
[12] L. Ji, Z. Lin, A.J. Medford, X. Zhang, Chemistry: A European Journal 15 (2009) 10718–10722.
[13] Z. Lin, L. Ji, M. Woodroof, X. Zhang, Journal of Power Sources 195 (2010) 5025–5031.
[14] B. Guo, Y. Li, Y. Yao, Z. Lin, L. Ji, G. Xu, Y. Liang, Q. Shi, X. Zhang, Solid State Ionics 204 (2011) 61–65.
[15] X. Liu, Z. Huang, S. OH, P. Ma, P.C.H. Chan, G.K. Vedam, K. Kang, J. Kim, Journal of Power Sources 195 (2010) 4290–4296.